Environmental Modelling and Software 143 (2021) 105109

Contents lists available at ScienceDirect

Environmental Modelling and Software

journal homepage: www.elsevier.com/locate/envsoft

Physical and numerical modelling of air-water flows: An Introductory Overview

C. Gualtieri [a,*], H. Chanson [b]

[a] University of Napoli Federico II, Napoli, Italy
[b] The University of Queensland, School of Engineering, Brisbane QLD, Australia

ARTICLE INFO

Keywords:
Air-water flows
Introductory overview
Physical modelling
Numerical modelling
Metrology
Model validation

ABSTRACT

In free-surface turbulent flows, large amount of air may be entrapped and advected in the water current. The resulting air-water flows are frequently observed in natural water systems, where they are also relevant to water quality, ecological sustainability and integrated assessment within such systems. Herein, a review of physical and numerical modelling of air-water flows is developed, providing some fundamentals towards a consistent modelling of such flows to graduate and Ph.D. level students as well as young researchers in environmental sciences and engineering, with pre-requisite knowledge in basic fluid mechanics. After some theoretical and metrology considerations, the main criteria for the design of physical models and the current literature on the numerical studies are discussed. Two case-studies, the hydraulic jump and the dropshaft, are used to show the application of such criteria and methods. Overall, the paper presents current knowledges/challenges on physical and numerical modelling of self-aerated free-surface flows.

1. Introduction

In high velocity free-surface turbulent flows, large quantities of air bubbles/pockets move across the air-water interface being entrapped (air entrainment) in the water current and then are carried away within the flowing fluid and, eventually, exchanged back to the air flowing above the free-surface (Halbronn et al., 1953; Jevdjevich and Levin, 1953). The resulting air-water flow, or self-aerated flow, is a mixture of air and water consisting of both air packets within water and water droplets surrounded by air (Chanson, 1997).

Aerated flows are encountered in a wide range of applications in chemical, civil, environmental, mechanical, mining, nuclear and water engineering (Rao and Kobus, 1974) (Fig. 1). They span from small scale to very large-scale. In water and environmental systems, self-aerated flows are often observed in mountain streams, storm waterways, culverts, dropshafts, spillway chutes, tidal channels and stilling basins, where aeration is largely un-controlled (Wood, 1991) and such flows are also relevant to the water quality, sediment transport, ecological sustainability and, ultimately, environmental integrated assessment within such systems. Depending upon the application, air entrainment should be maximised, minimised or prevented (Wood, 1985).

The exchange of air across the air-water interface is driven by the turbulence next to the air-water interface. The free-surface breakup and air entrainment occur when the turbulent shear stress is greater than the surface tension force per unit area resisting the interfacial breakup (Hino, 1961; Ervine and Falvey, 1987). Once some air is entrained within the bulk of the flow, the break-up of air pockets occurs when the tangential shear stress is greater than the capillary force per unit area (Chanson, 2009). As bubbles and droplets are advected by the flow, particle collisions may lead to their coalescence, while air detrainment due to buoyancy also takes place. The complex interactions between the entrained air and turbulence may produce some bubble clustering. A cluster of bubbles is defined as a group of two or more bubbles with a distinct separation from the other bubbles before and after the cluster. Past studies demonstrated that a clustering analysis may provide some relevant insights about the interaction between turbulence and bubbly flow (Gualtieri and Chanson 2010, 2013; Wang et al., 2015a).

Traditionally, aerated flows are experimentally investigated through physical modelling, but more recently numerical studies have been carried out. Physical models for such experimental studies must be designed on a sound similitude. Otherwise, scale effects may affect the extrapolation of experimental results to full-scale prototype structures (Kobus, 1984). Aerated flows are commonly studied using a Froude similitude, but, in a geometrically similar model, the dynamic similitude

* Corresponding author.
E-mail address: carlo.gualtieri@unina.it (C. Gualtieri).

https://doi.org/10.1016/j.envsoft.2021.105109
Accepted 3 June 2021
Available online 12 June 2021

involves other dimensionless parameters. Shear flows are dominated by viscous effects, while the mechanisms of bubble breakup and coalescence are controlled by surface tension forces (Chanson and Gualtieri, 2008). Hence, dynamic similitude in aerated flow requires that Froude, Reynolds and Morton numbers should be identical in both the prototype and its model. But this is impossible to achieve using geometrically similar models unless working at the full-scale. Using the same fluids, i.e. air and water, in the prototype and in laboratory, a Froude and Morton similitude can be implemented, but the model Reynolds number cannot be as large as in the prototype, leading to viscous-scale effects in small-size models (Rao and Kobus, 1974; Wood, 1985; Chanson, 2009).

More recently, Computational Fluid Dynamics (CFD) methods have been applied to improve the current knowledge about self-aerated flows. Such methods were developed over 50 years ago by engineers and mathematicians to solve flow problems in the area of industrial engineering and their application was later extended to many areas of fluid dynamics, such as environmental fluid mechanics and water engineering, including aerated flows (Cushman-Roisin et al., 2012; Rodi, 2017). The main advantages of such methods are that they allow full control over the boundary conditions, that they provide data in every point of the computational domain simultaneously and they might be performed at full scale, albeit at a computational cost. CFD also allows efficient parametric analyses of different configurations and for different flows and environmental conditions. On the other side, CFD methods are generally affected by uncertainties about input parameters that should be carefully considered (Blocken and Gualtieri 2012). In self-aerated flows, further sources of uncertainty are related to the stability and sharpness of interfaces in schemes where interfaces are explicitly modelled, and in other schemes, to the representation of forces between the phases, such as the lift and drag exerted by particles, and to mesh refinement being limited by the particle size (Bombardelli 2012; Viti et al., 2018). Hence, CFD studies must be carried out following strict guidelines (Rizzi and Vos 1998; Roache, 1998, 2008; ASME, 2009) otherwise their accuracy and reliability and the correct use of their results can easily be compromised. Furthermore, the results of numerical studies require to be validated using high-quality experimental data collected in physical models. For aerated flows, several CFD techniques were applied, but in many cases the validation of CFD simulations were conducted in terms of flow depth, possibly time-averaged velocity, rarely including any comparison of void fraction distributions and interfacial properties (Chanson and Lubin, 2010; Viti et al., 2018), while, to get a comprehensive validation turbulent, microscopic flow quantities should also be considered.

This paper presents a review at the introductory level of physical and numerical modelling of aerated flows. The review is intended to provide fundamentals towards a consistent modelling of such flows to graduate and Ph.D. level students as well as young researchers in environmental sciences and engineering, with pre-requisite knowledge in basic fluid mechanics. First, after some theoretical considerations, including the metrology of air-water flows, the main criteria for the design of physical models are discussed. Then, the most widely used methods for the numerical simulation of aerated flows are presented and the current literature is reviewed pointing out the need for a proper validation of any numerical study. Two case-studies, the hydraulic jump and the dropshaft, which probably received the largest and the lower attention within the literature, respectively, are used to provide guidelines for the application of such criteria and methods. Finally current challenges and future outlook on self-aerated free-surface flows are discussed.

2. Basic considerations

2.1. Presentation

Incompressible turbulent flows are governed by the equations of conservation of mass and momentum. These laws are represented through the Navier-Stokes equations, which, in their original form, encompass all known internal and external effects of the motion of a fluid. Unlike single-phase turbulence, where even simple Reynolds closure models have proven some usefulness, simple models have failed by and large in the case of multiphase gas-liquid flows (Elgobashi 1991;

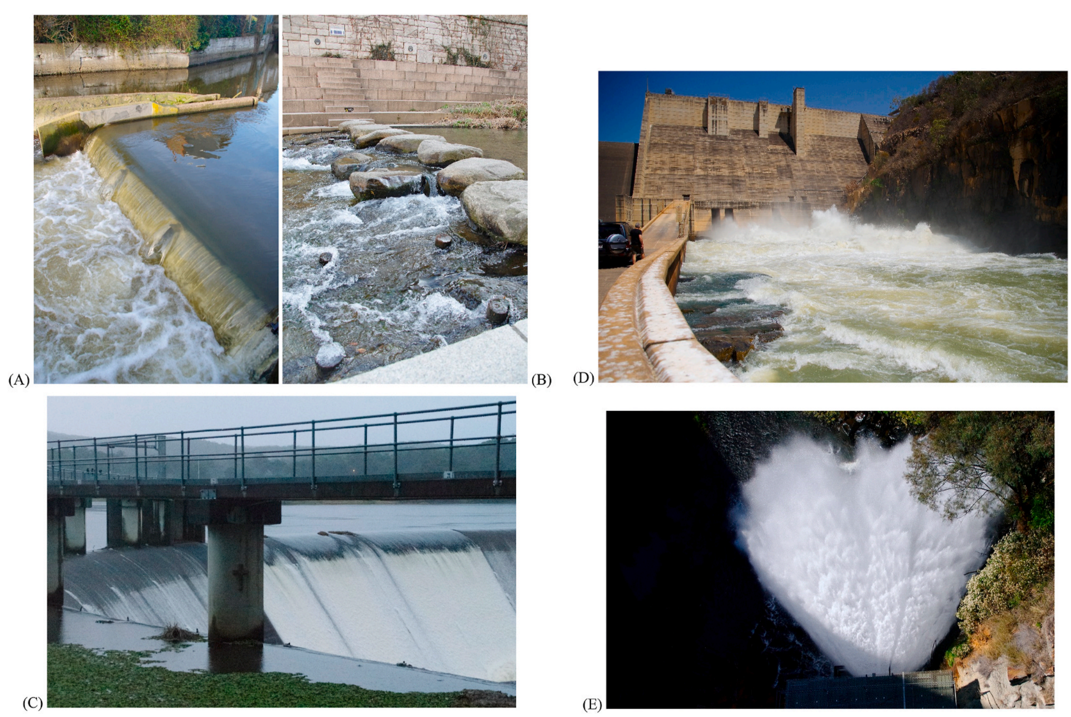

Fig. 1. Photographs of air entrainment in free-surface flows (Photographs Hubert Chanson) - (A) Nappe flow, plunging jet and hydraulic jump along Le Gouessant River at Lamballe, France on 30 December 2019; (B) Self-aeration at a man-made storm waterway canal at Dongdaemun, Seoul, Korea, on 13 January 2020; (C) Self-aerated flow chute flow on Wappa dam spillway, Sunshine Coast, Australia on 27 June 2018 ($q \approx 0.14$ m^2/s, Re $\approx 5.6 \times 10^5$); (D) Outlet air-water flows at Burdekin Falls dam, Australia on 16 November 2019; (E) Top view of bottom outlet at Moogerah dam, Australia on 28 September 2019 (outlet velocity $\sim$ 25 m/s).

Balachandar and Eaton, 2010). The complexity of the two-phase flow motion may be illustrated by the equations of fluid motion governing the multiphase gas-liquid flows at the micro-scale, combined with some interface tracking (Tryggvason et al., 2011; Bombardelli, 2012; Chanson, 2013):

$$\frac{\partial \rho_w}{\partial t} + \sum_{i=x,y,z} \frac{\partial (\rho_w v_{w_i})}{\partial x_i} = 0 \; Water \tag{1a}$$

$$\frac{\partial \rho_a}{\partial t} + \sum_{i=x,y,z} \frac{\partial (\rho_a v_{a_i})}{\partial x_i} = 0 \; Air \tag{1b}$$

$$\frac{\partial (\rho_w v_{w_i})}{\partial t} + \sum_{j=x,y,z} \frac{\partial (\rho_w v_{w_i} v_{wj})}{\partial x_j} = -\frac{\partial p_w}{\partial x_i} + \rho_w g_i + \sum_{j=x,y,z} \frac{\partial \tau_{w_{ij}}}{\partial x_j} \; Water \tag{2a}$$

$$\frac{\partial (\rho_a v_{a_i})}{\partial t} + \sum_{j=x,y,z} \frac{\partial (\rho_a v_{a_i} v_{aj})}{\partial x_j} = -\frac{\partial p_a}{\partial x_i} + \rho_a g_i + \sum_{j=x,y,z} \frac{\partial \tau_{a_{ij}}}{\partial x_j} \; Air \tag{2b}$$

where the subscripts a and w refer to the air and water properties respectively, v is the instantaneous velocity component, p is the instantaneous pressure, g_i is the gravity acceleration in the direction i = x,y,z, and τ_{ij} denotes an instantaneous shear stress tensor component. Equations (1a) and (2a) for the water, and Equations (1b) and (2b) for the air phase, must be complemented by a mathematical representation of the moving interface and the associated conditions to couple the equations across the air-water interfaces. This formulation may be used for detailed direct numerical simulations, although the application is very complicated (Prosperetti and Tryggvason, 2009; Tryggvason et al., 2011; Mortazavi et al., 2016). The interface tracking, the coupling of equations at the air–water interfaces and the correct implementation of the boundary conditions are "*not as easy as it may sound in engineering applications*" (Bombardelli, 2012).

Water crashing in high-velocity free-surface flows can be an extremely violent motion, with much spray and splashing, and complicated interfacial processes (Fig. 1). The generation of bubble clouds and water droplets has been proved to induce energy dissipation and turbulent mixing, to contribute to heat exchange, and to enhance gas transfer (Gualtieri and Gualtieri, 2004; Wanninkhof et al., 2009; Veron, 2015). Most recent modelling attempts are struggling with the lack of physical knowledge and conceptual model of the finest details of the breaking processes, which makes the task of parameterising the impact of self-aeration in steady and unsteady flows very difficult since no universal scaling laws for physical variables have been found so far (Lubin and Glockner, 2015; Lubin and Chanson, 2017). Newer models still need validation and further improvements.

2.2. Onset of air entrainment

The onset of self-aeration may be defined as the threshold condition for air entrainment to take place. Despite some fine distinction between the first single bubble entrainment and the onset of continuous bubble entrainment (e.g. Cummings and Chanson, 1999; Chanson and Manasseh, 2003), these two flow conditions usually cover a narrow range, broadly called the *onset of air entrainment*. Many early studies of air-water flows expressed the onset condition as a function of a time-averaged inflow velocity V_1, i.e. with air entrainment in turbulent water flows occurring for $V_1 > 0.5$–2 m/s (Rao and Kobus, 1974; Ervine et al., 1980). Some seminal studies related self-aeration to the inflow turbulence (Hino, 1961; Mckeogh and Ervine, 1981). More recently, detailed experimental studies showed a characteristic trend, with onset conditions about $V_1 \sim 2$ m/s in smooth turbulent flows and $V_1 \sim 0.8$ m/s in rough turbulent flows (Cummings and Chanson, 1999; Kiger and Duncan, 2012).

Nowadays, it is understood that air bubble entrainment occurs when the turbulent shear stress next to the free-surface interface is large enough to overcome the surface tension (Ervine and Falvey, 1987; Chanson, 2009). That is, the onset of air bubble entrainment is linked to a characteristic threshold in terms of Reynolds stresses, in the liquid phase, next to the air-water interface. For a spherical bubble of radius r, and isotropic turbulence, Chanson et al. (2021) derived an analytical expression of the onset condition:

$$\frac{\mu_w V}{\sigma} > \sqrt{\frac{\mu_w^{\,2}}{2\,\rho_w\,\sigma\,\pi\,r\,\frac{|vv|}{V^2}}} \tag{3}$$

where ρ_w is the water density, μ_w is the water dynamic viscosity, σ is the surface tension, V is the longitudinal water velocity, v is the instantaneous turbulent velocity fluctuation.

Despite the simplified development (spherical bubble, isotropic turbulence), Eq. (3) predicts entrained bubble sizes consistent with experimental data in vertical plunging jets (Chanson et al., 2021, Fig. 2).

2.3. Advection and turbulent diffusion of air bubbles

Once entrapped, the entrained air is carried away with the flowing fluid and its motion in within the water column is controlled by the complex interaction among advection, turbulent diffusion and mixing, and upward buoyancy. Furthermore, as bubbles and droplets are transported with the flow, turbulent shear may induce breakup and formation of smaller "daughter" particles, while particles collisions may lead to their coalescence. Various diffusion models were developed and applied successfully to a range of air–water flow typology and flow conditions (Chanson, 1997). In the hydraulic jump, the transport of air bubbles downstream the jump toe can be modelled using the classical advection-diffusion equation (Wood, 1984), where advection is along the horizontal direction and the diffusion process occurs only in the vertical direction (Chanson, 1995; 2010; Gualtieri and Chanson, 2007). In the dropshaft, the longitudinal distribution of air bubbles around the underwater jet trajectory follows the diffusion equation (Gualtieri and Chanson, 2004). The same type of equations can be applied even in other air-water flows such as on steep chutes and in vertical plunging jets (Chanson, 2012).

2.4. Air-water flow measurements

Air-water flows are usually investigated in the flow region where the air concentration is less than 95% and the two phases move with a nearly identical velocity (Chanson, 1997). For their description, in

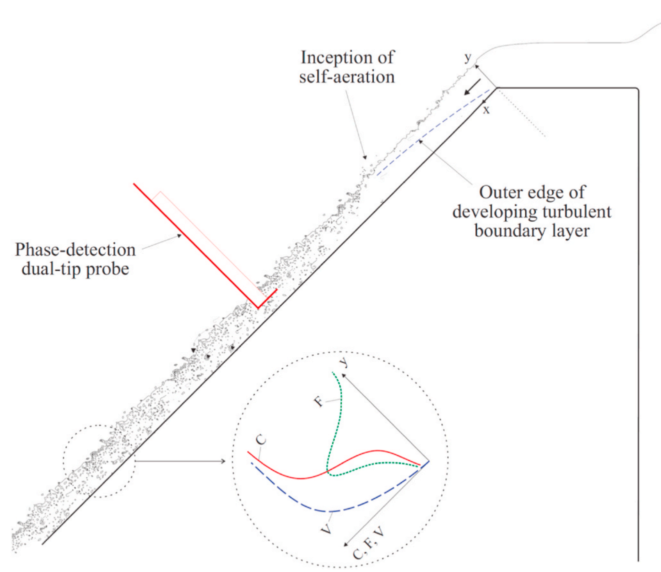

Fig. 2. Air entrainment down a steep chute.

comparison to a single-phase flow, aerated flows require a number of additional parameters, such as the air concentration or void fraction, the bubble count rate, the bubble and drop size distributions, the properties of clusters of air bubbles. Further, if void fraction exceeds 5%, some classical parameters of a turbulent flow, e.g. the instantaneous velocity, cannot be measured with traditional instruments, such as Pitot tube, acoustic Doppler velocimetry (ADV), laser Doppler velocimetry (LDA), because air bubbles and air-water interfaces affect adversely their operation.

Since the 1950s, some specialised instrumentations, such as back-flushing Pitot tubes, needle phase detection probes, conical hot-film probes and fibre phase Doppler anemometry, were developed for the measurement of aerated flows. However, their application was limited by calibration issues, and hence, the most widely applied device in the last 40 years has been the phase-detection needle shaped probe or conductivity probe, which is designed to pierce the bubbles and droplets (Fig. 3). Later, with the development of image-based velocimetry (particle image velocimetry, PIV) due to the advancement in computational power, bubbles were used as tracer particles under ordinary lighting conditions to identify velocity in aerated flows in a method called bubble image velocimetry (BIV). More recently, in the last decade, two major developments in air-water velocity measurements have been the total pressure probe and the Optical Flow (OF) metrology.

The needle probe is an intrusive phase-detection probe used to discriminate between air and water phases using the different conductivity of air and water. The signal output quality of this probe is closely linked to the sensor size, with the needle diameter, the sampling rate F_{sampl} and sampling duration T_{sampl}. Sensor sizes in less than 0.1 mm are used at low flow velocities ($V < 1$–2 m/s), while for higher velocity flows more sturdy probes with diameters typically between 0.1 and 0.5 mm are required. With a needle probe, the selection of the sampling frequency is linked to the smallest detectable bubble size, which is of the order of magnitude of the needle diameter. Generally, the sampling rate should be greater than 10 kHz and the sampling duration larger than 20 s to have negligible effect on the void fraction, bubble count rate and air–water velocity measurements, while more advanced correlation analyses, including the estimate of the turbulence intensity, require a sampling duration of 45 s or larger. The phase-detection probe could have a single-tip or a dual-tip design (Fig. 3B), where the latter provides additional information on the interfacial velocity and turbulence level.

Bubble image velocimetry (BIV) relies upon interrogation of an image frame pair by computing the spatial cross-correlation (Ryu et al., 2005). However, due to its discrete data nature, for certain tracer size range, the method may cause displacement vectors to be biased towards integer pixel values, commonly referred to as 'pixel locking' (Chen and Katz, 2005). Direct computation of the correlation surface is expensive and any velocity or seeding gradient in the interrogation region (especially a large region) introduces a bias towards smaller displacement. Another major limitation is the bias of the sidewall flow conditions, where boundary friction cannot be neglected. BIV velocity data typically underestimates the velocity field on the channel centreline, which is significantly larger than the near wall velocities when measured by an intrusive probe (Zhang and Chanson, 2018).

Total pressure measurements with miniature diaphragm sensor can deliver a fine characterization of the velocity and turbulence in the water phase, when accounting for the local void fraction (Wang et al., 2015b; Zhang et al., 2016).

The optical flow approach is based upon the detection of changes in brightness due to reflectance difference associated with passages of air-water interfaces (Bung and Valero, 2016a; Zhang and Chanson, 2018) (Fig. 6). Bung and Valero (2016b) compared BIV and optical flow estimates in seeded and aerated flows: they found comparable accuracies for both methods, with the optical flow technique providing higher resolution data albeit requiring a much longer computation time. Some key limitations of all optical techniques are the requirements for two-dimensional flows, the use of high-speed high-resolution video camera, and the adverse impact of sidewall effects (Bung and Valero, 2016a; Zhang and Chanson, 2018).

3. Similitude and physical modelling

Any modelling investigation is expected to deliver a sound prediction of the hydrodynamic characteristics of the flow motion in a full-scale prototype operation, with a few examples illustrated in Fig. 1 (Henderson, 1966; Hamill, 1995; Chanson, 2004a). The modelling approach must be developed based upon the basic principles of similitude, to deliver reliable extrapolations (Rayleigh, 1915). The presentation of any modelling data has to be relevant to the full-scale prototype applications, and dimensional analysis is the underlying method to deliver the most relevant design parameters (Bertrand, 1878; Rouse, 1938; Liggett, 1994). In air-water flows, an early study highlighted that "*Model tests provide little help due to our ignorance of the laws of hydrodynamic similarity of aerated flow*" (Jevdjevich and Levin, 1953, p. 439), while a more recent review paper emphasized that "*the results of experimental investigations demonstrated unequivocally the limitations of dynamic similarity and physical modelling of aerated flows*" (Chanson, 2013, p. 229). Yet, physical modelling and laboratory experiments remain essential tools to validate phenomenological, theoretical and numerical models (Hanratty et al., 2003).

In a study of self-aerated free-surface flows, the relevant dimensional parameters include the air and water properties, physical properties, channel dimensions, and inflow conditions. For a chute flow (e.g. Figs. 1C & 2), a simple dimensional analysis yield

$$C, V, v, F, N_c, L_t, T_t\ldots = F_1(x, y, z, \rho_w, \mu_w, \sigma, g, q, B, k_s, \theta, \ldots) \tag{4}$$

with C the void fraction, V the interfacial velocity, v a characteristic velocity fluctuation, F the level of flow fragmentation, N_c the cluster rate, L_t and T_t some characteristics turbulence length and time scale, x, y, z being respectively the longitudinal, normal and transverse co-ordinates, ρ_w the water density, μ_w the dynamic viscosity of water, σ the surface tension between air and water, g the gravity acceleration, q the unit discharge, B the channel width, k_s is the equivalent sand roughness height of the invert surface, and θ the chute slope.

The Buckingham Π theorem ([1]) states that any dimensional equation with N variables with units encompassing mass, length and time (MLT) may be rewritten into an equation with (N - 3) dimensionless parameters (Vaschy, 1892; Buckingham, 1914; Rouse, 1938). Thus, Equation (4) may be transformed as:

$$C, \frac{V}{V_c}, \frac{v}{V_c}, \frac{F \times d_c}{V_c}, \frac{N_c\, d_c}{V_c}, \frac{L_t}{d_c}, \frac{T_t\, V_c}{d_c}\ldots = F_2\left(\frac{x}{d_c}, \frac{y}{d_c}, \frac{z}{d_c}, \frac{d_c}{k_s}, \rho\frac{V\, D_H}{\mu}, \frac{g\,\mu^4}{\rho\,\sigma^3}, \frac{B}{d_c}, \theta, \ldots\right) \tag{5}$$

with d_c and V_c the critical flow depth and velocity respectively, and D_H the hydraulic diameter. Equation (5) expresses the local dimensionless air-water flow properties at a location (x,y,z) as functions of a number of dimensionless parameters, including the Froude number (4th term on the right handside), Reynolds number (5th term) and Morton number (6th term).

A laboratory study is typically undertaken using geometrically similar models. In the physical model, the air-water flow properties must display similarity of form, of motion and of forces (Novak and Cabelka, 1984; Chanson, 2004a). If this is not achieved, scale effects occur in relation to the parameter(s) of interest and the extrapolation of the model data will not accurately predict the full-scale prototype performances. Considering a high-velocity self-aerated flow in a rectangular channel (Figs. 2–5), the present analysis illustrated the large number of

[1] The Buckingham Π theorem is also called Vaschy-Buckingham theorem after the French engineer Aimé Vaschy (1857–1899) and American physicist Edgar Buckingham (1867–1940).

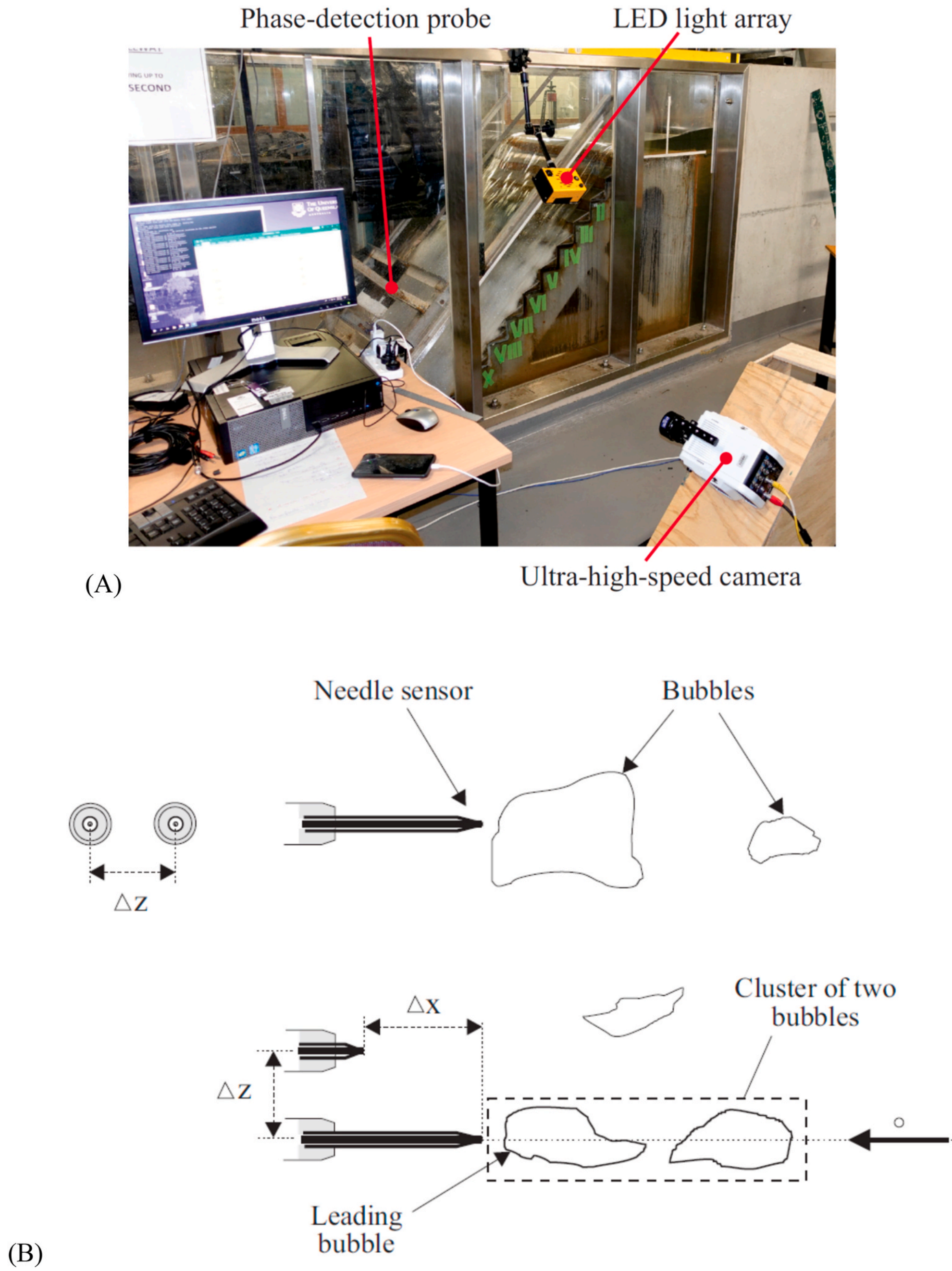

Fig. 3. Air-water flow measurements in a stepped spillway model at the University of Queensland - (A) Ultra-high-speed camera (sideview) for optical flow measurements and phase-detection probe on channel centreline; (B) sketch of bubble detection by dual-tip phase-detection probe (front view, side view, top view).

relevant parameters. Any true similarity would require identical dimensionless variables, including Froude, Reynolds and Morton numbers, in both laboratory and full-scale prototype. This situation is physically impossible because of the large number of independent parameters (Eq. (5)).

Past experiences showed that small laboratory experiments drastically under-represented the air entrainment (Kobus, 1984; Chanson, 1997, 2009). Figs. 4 and 5 illustrates the air entrainment in two types of self-aerated flows. Each figure presents photographs of the flow at an identical Froude and Morton number, but different Reynolds numbers. For scale, the inflow depth was 0.097 m, 0.045 m and 0.027 m in Fig. 4A, B and 4C respectively. In Fig. 5A, the shaft was 0.755 m long and 0.763 m wide, while the shaft was 0.243 m long and 0.246 m wide in Fig. 5B. Both examples emphasized the scale effects in small-sized laboratory facilities operating at relatively small Reynolds numbers. In practice, the laboratory experiments must be conducted in a large-size facility operating at relatively large Reynolds numbers: typically $Re > 2 \times 10^5$ to 5×10^5.

4. Numerical modelling

Numerical methods are increasingly applied to improve the current knowledge about self-aerated flows. Despite their several advantages, the accuracy and reliability of the numerical approach are still of concern, and verification and validation studies are limited. It is widely recognized that the results of CFD simulations can be very sensitive to the wide range of computational parameters that have to be set by the user. The set-up of any numerical study is associated to uncertainties

(A)
(B)
(C)

Fig. 4. Hydraulic jumps with breaking roller (Fr = 2.1) (Photographs Hubert Chanson) - Comparison between laboratory experiments at different Reynolds numbers: (A) Re = 8.0 × 10^5; (B) Re = 2.52 × 10^5; (C) Re = 1.16 × 10^5 - Flow direction from left to right, note the phase-detection probe in Fig. 4A and B; Fig. 4B and C are respectively 1:2.1 and 1:4 scale model of Fig. 4A - In each photograph, the channel was 0.50 m wide and the sidewall height was 0.40 m.

about geometry and boundary conditions, drag coefficients, driving forces, and the interactions among different processes and inputs. This is of paramount importance in the numerical simulation of self-aerated flows, which involves fluctuating boundaries, as well as a multiphase flow.

While CFD methods were previously applied to self-aerated flows to supplement the use of physical models (Bombardelli, 2012) and address the intrinsic limitations of experimental measurements, the development of advanced theoretical models for turbulence and two-phase flows led such numerical methods to be often applied together with experimental methods to tackle and interpret self-aerated flows in the last decade.

A flow field may be described following two approaches: Eulerian methods and Lagrangian methods. The first approach studies flow properties in a number of fixed points. This corresponds to a coordinate system fixed in space, where fluid properties are studied as functions of time as the flow passes. The latter follows the motion of each individual fluid parcel as it moves from some initial location. This corresponds to a coordinate system on each fluid parcel. Past numerical simulations of aerated flows encompass both Eulerian, such as Reynolds-Averaged Navier-Stokes (RANS), Detached Eddy Simulation (DES), Large Eddy Simulation (LES) and Direct Numerical Simulation (DNS), and Lagrangian, such as Smoothed Particle Hydrodynamics (SPH), methods (Bombardelli, 2012; Rodi et al., 2013; Violeau and Rogers, 2016; Viti et al., 2018).

The most widely applied approach to simulate a turbulent flow is that based on the time averaging, even termed Reynolds-averaging, of the Navier-Stokes equations, where the instantaneous values of velocity and pressure is assumed to be the sum of a time-averaged value and a fluctuating component. This statistical approach leads to the Reynolds-Averaged Navier-Stokes (RANS) equations (Kundu et al., 2012), where the averaging of non-linear advective terms results in unknown correlations between fluctuating velocities. These additional unknowns introduce the need for a "*closure*" of the RANS equations. Such correlations are usually seen as stresses, termed Reynolds stresses, additional to those due to fluid viscosity. Following the Boussinesq hypothesis, Reynolds stresses are treated using an eddy (or turbulent) viscosity and the spatial gradient of the time-averaged velocities (Kundu et al., 2012). Such eddy viscosity ultimately means that the effect of turbulence is to act on the mean flow as an increased viscosity.

Different estimations for the eddy viscosity have been proposed. Dimensional reasoning suggests that the eddy viscosity can be obtained as a product of a turbulent velocity-scale by a turbulent length-scale. Different approaches can be used to derive these scales. At the simplest level of complexity, one may expect that the eddy viscosity would be determined by large-scale eddies, the size of which is close to the characteristic dimension and velocity of the flow itself. Thus, eddy viscosity would be linked to the overall velocity gradient as in the mixing length model (Kundu et al., 2012). Alternatively, an obvious choice for defining a turbulent velocity scale is the turbulent kinetic energy k, while many variants were proposed in the literature to define a turbulent length scale leading to different families of two-equations turbulence models, such as the k-ε model and the k-ω turbulence model, where the rate of turbulent energy dissipation ε and the specific dissipation rate $\omega=\varepsilon/k$, respectively, are used to get a turbulent length scale. Each of these families has different derived models characterised from different equations and numerical constants.

RANS approach has been frequently applied in aerated flows, such as the hydraulic jump (Chippada et al., 1994; Gonzalez and Bombardelli, 2005; Bayon et al., 2016; Valero et al., 2018; Witt et al., 2018, Macián-pérez et al., 2020), smooth and stepped spillways (Meireles et al., 2014; Toro et al., 2016; Lopes et al., 2017; Valero et al., 2018), chutes (Hohermuth et al., 2020), dropshafts (Sousa et al., 2009), and plunge pools (Carrillo et al., 2020). Often, in such studies, an additional method is required to track the free surface, i.e., Volume of Fluid (VoF) by Hirt and Nichols (2008). While the large scale of the turbulent spectrum produced by mean flow is long-living, energetic, diffusive, inhomogeneous, anisotropic and depending on domain geometry and boundaries, the small scale, produced by large eddies, is short-living, no-energetic, dissipative, universal, random, homogeneous, isotropic and can be modelled statistically (Rodi et al., 2013). This fundamental difference has led to conceptualize the Large Eddy Simulation (LES) approach, where the large scale of turbulence is resolved, while the small scale is modelled (Rodi et al., 2013). The main difference between RANS and LES approaches is that the Navier-Stokes equations are, in the former, time-averaged and, in the latter, space filtered. Furthermore, the cut-off, below which a model is used, is a frequency-domain cut-off in LES, whereas in RANS it is a physical-domain cut-off. In spite of that, both sets of equations get a similar form because a stress tensor is created by the time-averaging and filtering processes. However, in LES, differently from RANS models, these stresses, called sub-grid scale stresses, pertain only to the turbulent spectrum that is not solved but modelled

(A)  (B)

Fig. 5. Rectangular dropshafts (Photographs Hubert Chanson) - (A) 1:1 full-scale model (Regime R3); (B) 1:3.1 scale model (Regime R2) - Note the drastically lesser bubble cloud in the smaller model (Right) - In Fig. 5A, the shaft was 0.755 m long and 0.763 m wide, while the shaft was 0.243 m long and 0.246 m wide in Fig. 5B.

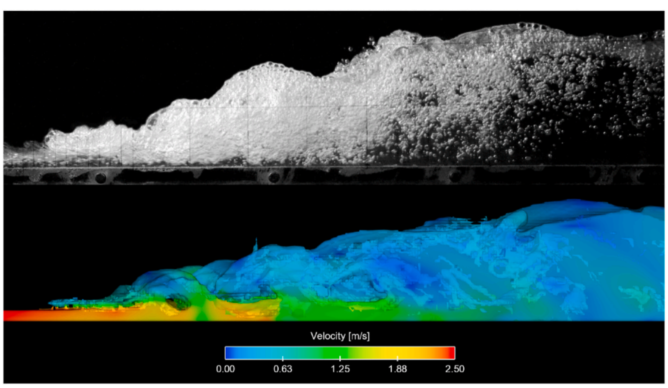

Fig. 6. Hydraulic jump with inflow Froude number about 6 (from Viti et al. (2018) - Flow from left to right - Top: experimental model (Valero et al., 2014); Bottom: numerical model (Bayon et al., 2016).

using different methods (Rodi et al., 2013). LES is more computationally demanding that RANS, but the continuous development of computational power has led LES approach to be increasingly applied to water engineering and environmental hydraulics, including to self-aerated flows, such as the hydraulic jump (Gonzalez and Bombardelli, 2005; Lubin et al., 2009) and tidal bores (Lubin et al., 2010a; 2010b; Leng et al., 2018a,b). To combine the advantages of RANS and LES, minimising their limitations, hybrid LES-RANS approaches, such as Detached Eddy Simulation (DES) were proposed and even applied to aerated flows, but to the hydraulic jump only (Ma et al., 2011; Jesudhas et al., 2018, 2020). Basically, in the DES, RANS and LES methods are used in the near-wall region and in the free-stream region respectively (Rodi, 2017).

In the Direct Numerical Simulation (DNS) the unsteady 3D Navier–Stokes equations are solved directly using spatial and temporal resolutions sufficiently fine to resolve the dynamics of the entire spectrum of turbulent eddies in the flow: from the energy-producing largest eddies, whose size is comparable to the flow domain, to the smallest eddies of Kolmogorov scale, at which turbulence energy is dissipated into heat by molecular action. It is easy to identify a critical issue for DNS in the extremely large computational power, in terms of both the processor's performances and the size of the memory for storing intermediate results required to achieve results for real-world problems in a reasonable time. It is noteworthy that the computational power needed by DNS is proportional to the flow Reynolds number $Re^{9/4}$. The contributions of DNS to turbulence research in the last few decades have been impressive (Alfonsi, 2011), but its application to water engineering and environmental hydraulics problems, which are characterised by large Reynolds numbers, is still very limited and in the field of self-aerated flows only a study on hydraulic jump (Mortazavi et al., 2016) was published so far.

Among the meshless Lagrangian techniques, Smoothed Particle Hydrodynamics (SPH), which solves flow equations for a set of moving particles (with a certain mass), has been recently applied to aerated flows, such as the hydraulic jump (López et al., 2010; De Padova et al., 2013, 2018; Wan et al., 2018), smooth and stepped spillways (Wan et al., 2017; Nobrega et al., 2020) and tidal bores (Nikeghbali and Omidvar, 2017). While the use of a kernel function to interpolate flow-variables is critical to SPH, some general advantages of the SPH method over the mesh-based methods are the effectiveness in solving complex fluid dynamic problems with highly nonlinear deformations and the natural tracking of free surfaces and moving boundaries.

The analysis of the above-mentioned literature shows that the number of numerical studies capable to gain a complete validation of their results is still limited. For the hydraulic jump, which is the most frequently investigated self-aerated flow, most RANS/LES/SPH studies focused on the free-surface simulation and on the prediction of the main jump parameters (conjugate depth ratio, roller length, hydraulic jump length and efficiency, etc.) and time-averaged velocity, while only few studies considered also pressure fluctuations, turbulence features and air entrainment quantities (void fraction). On the other side, high fidelity methods, such as DES and DNS, were extended to a comprehensive characterization of turbulence, including the identification of coherent structures and interface length scales, and of air entrainment (Mortazavi et al., 2016; Jesudhas et al., 2018, 2020) (Fig. 6). For smooth and stepped spillways, RANS studies gained mostly a characterization of average velocity and pressure distribution, vorticity, turbulent kinetic energy and its dissipation rate (Meireles et al., 2014; Toro et al., 2016), while SPH predicted flow depth and velocity (Nobrega et al., 2020) and also the longitudinal distribution of dissolved oxygen (DO) concentration (Wan et al., 2017). Numerical studies on tidal bores, both with LES and SPH, focused on the prediction of time-variable free-surface dynamics and velocity distribution (Lubin et al., 2010a; 2010b; Nikeghbali and Omidvar, 2017; Leng et al., 2020). Finally, while the numerical analysis of a dropshaft was limited to discharge and water depth (Sousa et al., 2009), very recent RANS studies on chutes (Hohermuth et al., 2020) and plunge pools (Carrillo et al., 2020) gained the prediction of both the velocity field and of air entrainment, including void fraction, bubble frequency and Sauter bubble diameter. In a highly transient flow, one application showed that the instantaneous void fraction and bubble distribution data presented systematically a lesser aeration region in the physical model, compared to the numerical data (Leng et al., 2018b).

5. Discussion

At the end, it is advisable for numerical studies of self-aerated flows to get a comprehensive validation across a broad range of relevant air-water flow properties, with relevant turbulent integral length and time scales in addition to the microscopic flow structure (e.g. clustering, interparticle distances), in line with the CFD validation requirements set for monophase flows (Rizzi and Vos, 1998; Roache, 1998; 2008; ASME, 2009; Blocken and Gualtieri, 2012).

The validation of CFD numerical models is anything but trivial. A proper validation necessitates a combined and fundamental understanding of the numerical model, and its limitations, together with an expert knowledge of the physical model, its characteristics, and its instrumentation (Leng et al., 2018a). Such a combined expertise and experience is critical to ensure the suitability of the experimental physical data set for CFD validation. Most often, a proper CFD model validation required a team of experts with physical and numerical experience. Yet both physical and numerical models are developed to reproduce a full-scale three-dimensional flow phenomenon, for which prototype data are rarely available for the ultimate validation (Chanson, 2013).

A recent development has been the hybrid modelling combining laboratory experiments and numerical Computational Fluid Dynamics (CFD) modelling together (Fig. 7) (Leng et al., 2018b; Leng and Chanson, 2020). A major advantage in engineering design is the optimisation of resources, combining the flexibility of CFD modelling, e.g. to reduce the costs in building and testing several large-size physical models, and operating large-size laboratory models to produce realistic boundary and initial conditions, yielding high-quality validation data sets for CFD numerical modelling, in turn reducing the total simulation times. Such a composite approach may include interactions, feedbacks and loops between the physical and CFD techniques, providing new capabilities to the entire design process.

5.2. Case studies

5.2.1. The hydraulic jump

A hydraulic jump is a sudden transition from a high-speed open channel flow into a slow fluvial flow, commonly experienced in streams and rivers, as well as in man-made canals, industrial channels and downstream of dam spillways. The jump is a seminal fluid flow, with extreme turbulence linked to the development of large-scale eddies, surface waves and spray, energy dissipation and air entrainment (Figs. 4 and 8). It is the most largely investigated (physically and numerically)

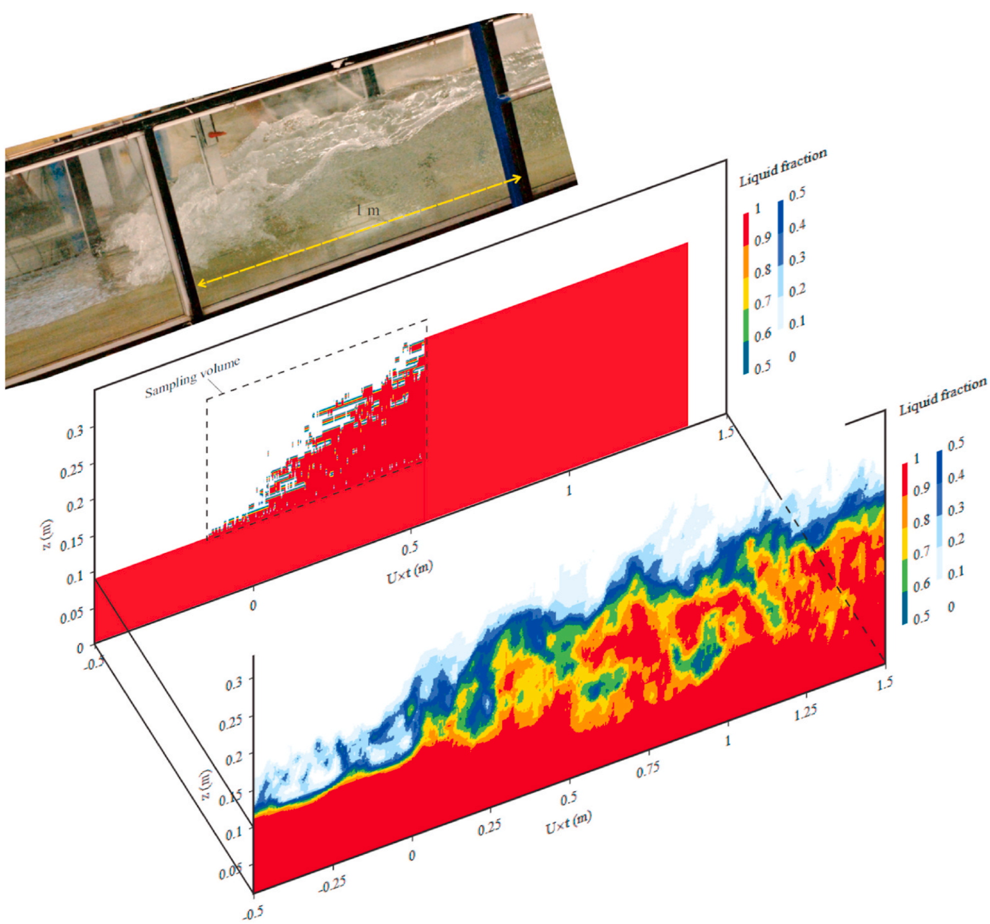

Fig. 7. Hybrid modelling of a breaking bore with surge front propagation from right to left: liquid fraction contour maps for $Fr_1 = 2.1$ (Leng et al., 2018b) - Foreground: CFD LES numerical modelling; Middle: physical modelling in a 19 m long 0.7 m wide channel; Background: photograph of physical model (shutter speed: 1/320 s).

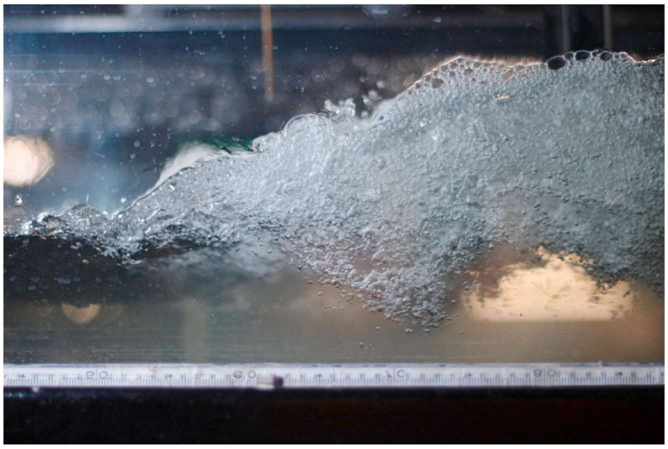

Fig. 8. Air entrainment in hydraulic jump (Photograph Hubert Chanson) - Flow conditions: $d_1 = 0.097$ m, $V_1 = 2.04$ m/s, Fr = 2.1, Re = 8×10^5, flow direction left to right, shutter speed: 1/1600 s.

self-aerated flow. In a hydraulic jump, some air is entrapped at the discontinuity between the impinging flow and roller, called jump toe or roller toe (Rajaratnam, 1962; Chanson and Brattberg, 2000; Murzyn et al., 2005). Further air is entrained through the roller free-surface (Wang and Chanson, 2015). At the jump toe, the impingement perimeter acts as a source of vorticity, and the developing air-water mixing layer is the locus of the advective diffusion of vorticity and entrained air.

The hydraulic jump is characterised a sudden rise in water levels (Figs. 4 and 8), associated with some discontinuity in terms of the pressure and velocity fields. It is a hydrodynamic shock (Lighthill, 1978; Liggett, 1994). The application of the equations of conservation of mass and momentum in an integral form gives a system of equations linking the one-dimensional flow properties upstream and downstream of the jump (Henderson, 1966; Chanson, 2012a). For hydraulic jumps in a smooth horizontal rectangular channel, it yields:

$$\frac{d_2}{d_1} = \frac{1}{2}\left(\sqrt{1 + 8\,Fr_1^2} - 1\right) \tag{6}$$

$$\frac{Fr_2}{Fr_1} = \left(\frac{2}{\sqrt{1 + 8\,Fr_1^2} - 1}\right)^{3/2} \tag{7}$$

where d and V are the flow and depth averaged velocity respectively (Fig. 9A), the subscripts 1 and 2 refer to the upstream and downstream conjugate properties, and Fr is the Froude number defined as: $Fr = V/(g \times d)^{1/2}$ for a rectangular channel. Equations (6) and (7) highlight the importance of the inflow Froude number Fr_1, and the selection of the Froude similitude for any physical modelling derives implicitly from these fundamental theoretical considerations.

A key feature of the hydraulic jump is the developing shear layer with a recirculation region above (Figs. 8 & 9A). The turbulent shear flow is somehow analogous to a wall jet (Rajaratnam, 1965; Chanson and Brattberg, 2000), while the advection of air bubbles can be modelled by an advection-diffusion equation (Chanson, 1995, 1997). Typical vertical distributions of void fraction C, bubble count rate F and longitudinal velocity V_x are sketched in Fig. 9B. The shear layer is typically characterised by a local maximum in void fraction C_{max}, which decreases pseudo-exponentially with increasing distance from the roller toe as the shear layer expands (Chanson and Brattberg, 2000; Murzyn et al., 2005). Similarly, some momentum consideration implies that the maximum velocity V_{max} decays quasi-exponentially with longitudinal distance from the roller toe. Typical experimental observations of C_{max} and V_{max} are shown in Fig. 9C, in which they are compared with two robust correlations (Wang and Chanson, 2016; Chanson, 2010):

$$C_{max} = 0.5\,\exp\left(-\frac{1}{1.8\,(Fr_1 - 1)}\;\frac{x - x_1}{d_1}\right) \tag{8}$$

$$\frac{V_{max}}{V_1} = \exp\left(-0.028\;\frac{x - x_1}{d_1}\right) \tag{9}$$

with x_1 the roller toe position.

The development of large turbulent structures and vortex pairing is conducive of bubble clustering in the turbulent mixing layer (Chanson, 2007a; Wang et al., 2015a) (Figs. 3 and 8). While a cluster is a three-dimensional air-water structure, the current metrology is restricted to the detection of longitudinal and transverse clusters. Experimental data showed a large proportion of entrained bubbles advected in clusters, typically mostly encompassing between 2 and 5 bubbles (Wang et al., 2015a).

During the past two decades, hydraulic jumps have been also investigated using numerical methods, both Lagrangian and Eulerian (Gonzalez and Bombardelli, 2005; Viti et al., 2018). Most numerical studies have been carried out by RANS approach to validate this tool for a set of flow conditions. Different two-equations turbulence models, mostly belonging to the *k-ε* family, were applied in a range of inflow Froude number from 1.5 to 9.5. Generally, RANS simulations yielded relatively accurate results, with accuracies over 90% for average flow variables (conjugate depth ratio, roller length, hydraulic jump length and efficiency, mean free-surface) and even, in some cases, for air entrainment, mainly investigated in terms of air concentration (void fraction), and not considering the distribution of bubbles sizes (Viti et al., 2018). At the end, any of the applied two-equation models presented could be used for design purposes provided that the related uncertainties are considered in the analysis of the numerical results. While meshless SPH simulations showed a promising agreement in terms of free surface elevations and velocity profiles, high fidelity methods, such as LES and, mostly, DES and DNS, provided a comprehensive characterization of turbulence quantities indicating the future area of development of numerical studies on the hydraulic jump (Mortazavi et al., 2016; Jesudhas et al., 2018, 2020).

5.2.2. *Air entrainment in a rectangular dropshaft*

A dropshaft is a vertical conduit connecting two channels located at different elevations (Figs. 5 and 10). The loss in potential energy acts basically as some energy dissipation. In practice, there are two common types of dropshaft, i.e. the plunge type and the vortex type. The plunge dropshaft design, herein investigated, has been used for millennia (Lopez-Cuervo, 1985; Chanson, 2002a), and modern applications encompass sewers, storm waterways, and even large spillway shafts with Morning Glory intake. However, the literature on dropshaft is not large. The dropshaft operation may cover several flow regimes, depending upon the boundary conditions, i.e. shaft geometry, and inflow conditions. Most frequently, flow and air entrainment in a dropshaft are investigated by physical modelling (Chanson, 2002a; 2004b; 2007b; Camino et al., 2015; Ma et al., 2016; Ding and Zhu, 2018), while numerical studies are unfortunately still limited (Sousa et al., 2009).

Let us consider a rectangular dropshaft, as illustrated in Figs. 5A and 10, which is a near-full scale facility. At low discharges, the free-falling nappe impacts into the shaft pool (Regime R1) (Fig. 10A) (Chanson, 2004b; Gualtieri and Chanson, 2004), while, at large flow rates, the nappe impacts on the opposite wall (Regime R3) (Figs. 5A & 10B) (Chanson, 2007b). For a narrow range of intermediate flows, the nappe impact may interfere with the shaft outflow conduit (Regime R2) (Fig. 5B). In the regime R1, the air entrainment is primarily a plunging jet action, with bubble entrainment occurring at the plunge point. At large discharges, air entrainment is a combined effect of nappe impact and splashing on the opposite wall, and plunging action in the shaft pool (Fig. 10). Air entrainment in such dropshaft was experimentally investigated using a sturdy single-tip phase-detection probe (Chanson, 2002b;

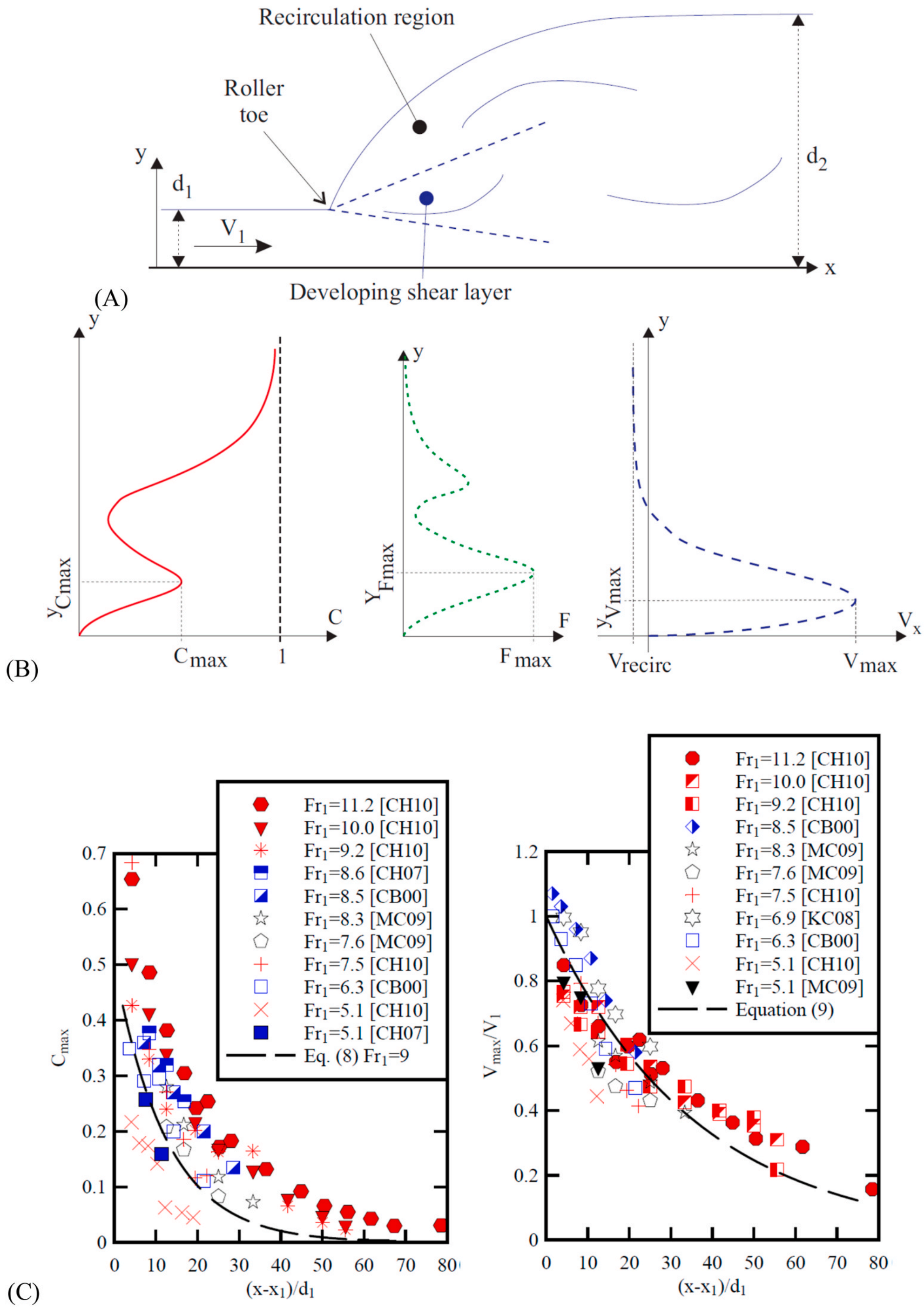

Fig. 9. Air entrainment in the shear layer of a hydraulic jump - (A) Sketch of a hydraulic jump with a marked roller; (B) Typical distributions of void fraction C (Left), bubble count rate F (Middle) and longitudinal velocity V_x in the roller (Left); (C) Longitudinal distribution of local maximum in void fraction C_{max} (Left) and maximum velocity V_{max} (Right) in the shear layer - Data sets: [CB00] Chanson and Brattberg (2000), [CH07] Chanson (2007a), [KC08] Kucukali and Chanson (2008); [MC09] Murzyn and Chanson (2009), [CH10] Chanson (2010).

2007b; Gualtieri and Chanson, 2004). Such laboratory experiments showed a strong aeration of the dropshaft pool for all discharges with entrained bubbles' mean size between 10 mm and 20 mm (Chanson, 2007b). Maximum void fraction was located close to the theoretical trajectory of underwater jet (Fig. 11A), where turbulent shear was the largest, but bubble coalescence and detrainment processes reduced the percentage of the smaller air bubbles along such trajectory. Furthermore, a decreasing number of air bubbles could penetrate into the pool at increasing depths. Void fraction data were found to obey to an analytical solution of diffusion equation for air bubbles, whose distribution was skewed and followed reasonably well a log-normal probability distribution function (Chanson, 2002b; 2007b; Gualtieri and Chanson, 2004).

Bubble clustering was further investigated in such dropshaft aerated flow to better characterise the interactions between bubbles and large-scale vortices. Bubble clusters can be identified by analysing the water chord between two adjacent air particles or the interparticle arrival times (IATs) τ_{IA} for the air bubbles. While the former method provides only some general features of the clustering process, such as the number of clusters, of clustered bubbles and of bubbles belonging to cluster structures in each point of measurement, the IAT analysis allows also to identify the range of particle sizes affected by clustering and ultimately the structure of each cluster and of the bubbly flow. Both methods demonstrated the relevance of clustering process in the dropshaft flow. Clustering was the largest close to the plunge point in the pool and along the theoretical trajectory of underwater jet with some decaying pattern

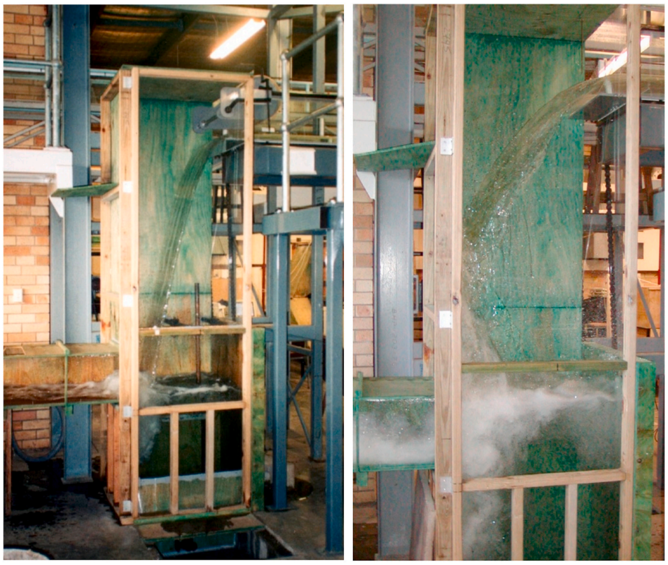

Fig. 10. Air entrainment in a large rectangular dropshaft (Photographs Hubert Chanson) - (A, Left) Re = 2.4×10^5, drop in invert elevation: 1.7 m (Regime R1); (B, Right) Re = 4×10^5, drop in invert elevation: 1.7 m (Regime R3).

with the depth (Gualtieri and Chanson, 2011, 2013). The IAT data demonstrated that, for a similar level of turbulence, the bubbly flow structure in the dropshaft had a density of bubbles per unit flux larger than in the hydraulic jump flow (Fig. 11B), suggesting a stronger level of interaction between air bubbles and turbulent flow in the dropshaft (Gualtieri and Chanson, 2013).

As already noted, numerical studies of the above presented rectangular dropshaft are mostly limited to that of Sousa et al. (2009). Sousa and co-workers investigated the hydraulic operation in that dropshaft using both standard k-ε and RNG k-ε turbulence models combined with the VoF (Volume of Fluid) method for tracking and locating the free-surface. Their numerical results were compared with the experimental data by Chanson (2002b) demonstrating a reasonable agreement in terms of discharge and water depth. Future numerical studies should gain a more comprehensive characterization of the dropshaft flow, including air entrainment and bubble clustering.

6. Conclusion and outlooks

High-velocity free-surface flows are characterised by a sizeable amount of entrapped air, and the advection of air-water structures interacts with both the flow turbulence and atmosphere. These self-aerated flows are complicated multiphase flow motions, commonly observed in natural water systems, including breaking waves, torrents and bores, as well as in hydraulic structures. The 'white waters' have direct implications onto the water quality, ecological sustainability and environmental integrated assessment of the natural systems. In this Introductory Overview of physical and numerical modelling of self-aerated air-water flows, the authors aimed to deliver a fundamental understanding to assist graduate and PhD level students, as well as early career professionals, with the modelling of self-aerated flows. Two case-studies of self-aerated flows, the hydraulic jump and the dropshaft, were introduced to illustrate the challenges in modelling air-water flows.

So, what is so special about self-aerated air-water flows? They are multiphase, i.e. gas-liquid. The basic equations must be developed for both phases, with some coupling equations at the air-water interfaces. The interactions between air-water entities and turbulent structures are not trivial, and the use of standard force laws, and mass- and momentum-transfer correlations, typically developed for single-phase flows, can result in significant errors. Simply, the influence of turbulence on the entrained air and surrounding atmosphere cannot be ignored. This is sometimes referred to as 'two-way coupling' or even 'four-way coupling' between the various phases.

The presence of air-water interfaces has some direct implication in the measurement techniques and instrumentation used in laboratory and prototype. Traditional instruments, e.g. Pitot tube, PIV, LDA, are adversely affected by the gas-liquid interfaces. Despite recent progresses in optical techniques, the sidewall boundary effects cannot be neglected, and the most robust metrology in highly self-aerated free-surface flows is the needle phase-detection probe. Another challenge in physical modelling is the well-known scaling issue with small-size laboratory experiments. Small laboratory models drastically underestimate the air entrainment, and the physical results cannot be extrapolated to a full-scale system without bias and errors, i.e. scale effects.

The multiphase structure of the flow impacts directly on the selection of suitable computational models. Several approaches were tested, including RANS, LES, DES, DNS and SPH. Such CFD studies were mostly applied to the hydraulic jump, with a few applications to smooth and stepped spillways, breaking bores, dropshafts and plunge pools. A seminal challenge is the validation of the CFD results, because it requires detailed air-water physical data sets. The quality of the validation data

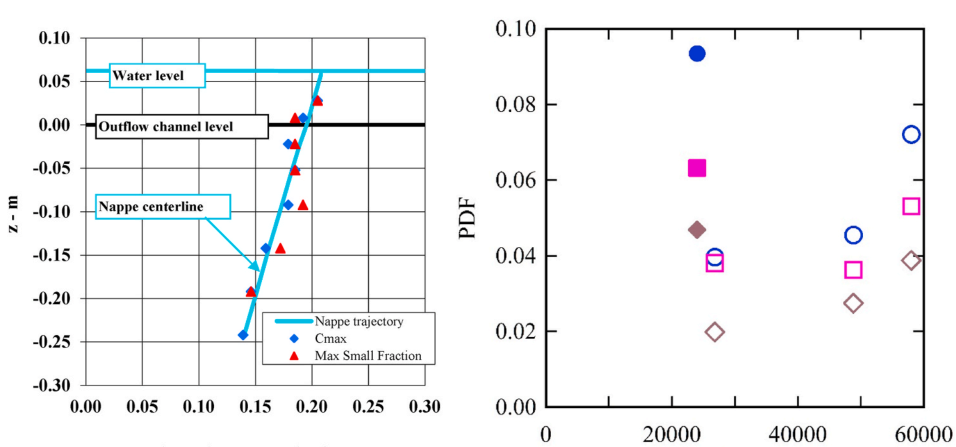

Fig. 11. (A) Calculated underwater jet trajectory with the x-locations of maximum void fractions, i.e. C_{max}, at each depth z (Gualtieri and Chanson, 2004); (B) Distribution with Re of the PDF in the dropshaft (full symbols) and in the hydraulic jump (empty symbols) for bubbles with τ_{IA} from (● and ○) 0–0.5 ms (■ and □) from 0.5 to 1.0 ms and (◆ and ◇) from 1.0 to 1.5 ms (Gualtieri and Chanson, 2013).

sets must be scrutinised, because "*the validation process at the highest stage relies on comparisons with experiments*" (Rizzi and Vos, 1998, p.669). What type of data, e.g. void fraction, interfacial velocity, bubble size distributions? Are turbulent multiphase flow quantities at the millimetric and sub-millimetric scales (e.g. clustering, interparticle distances) needed for a proper validation of CFD studies? With what accuracy such validation should be carried out? How confidently can the physical data set be extrapolated to a full-scale prototype? How could the results of CFD studies be applied to the design of hydraulic structures in water engineering? The authors want to stress, in the strongest terms, the uppermost importance of CFD validation "*because nature is the final jury*" (Roache, 1998, p. 697).

What are the outlooks? On one side, the last decade has seen some major development in air-water self-aerated flows. Detailed physical modelling studies are more common, with a substantial increase in the amount of advanced air-water flow measurements, with needle phase-detection probes, optical techniques and other multiphase flow instrumentation. Advanced CFD research showed promising results with early DNS work and even DES simulations, although most studies are still based upon LES and RANS. Meshless Lagrangian SPH method was also recently applied to self-aerated flows. It should be expected that the continuous increase in the available computational resources and modelling techniques will promote a shift of the applied CFD methods towards high-fidelity approaches, such as LES and DNS. A very recent and successful development has been the hybrid modelling, combining parallel physical and CFD numerical modelling, with two-way interactions between the two modelling techniques. Altogether we believe beyond doubt that all these recent progresses have been tremendous.

On another side, there still some major knowledge gaps. Three obvious issues are (1) a lack of full-scale prototype data, (2) the requirements for high-quality detailed validation data sets for CFD model development, and (3) the need to expand modelling to more complicated air-water flow applications. New field measurements, performed in situ, constitute a key requirement to corroborate physical laboratory data and substantiate current CFD validation approaches based upon laboratory validation sets. Let us remember that even the large dropshaft, seen in Figs. 5A and 10, could be regarded as a scale model of the larger dropshafts built beneath the cities of Tokyo and Chicago, for example. In physical modelling, it is extremely difficult, if not impossible, to access detailed information at all spatio-temporal scales relevant to CFD modelling. Any physical modelling can only generate a limited number of variables, in contrast to numerical simulations which offer a larger range of outputs. Hence any validation contains intrinsic limitations. Simply let us remember that the validation of CFD numerical models is not trivial! Finally, many practical applications correspond to some complicated three-dimensional multiphase flow (Fig. 1), that current physical and numerical models are most often unable to predict accurately. Most detailed physical models are two-dimensional, and three-dimensional validation data sets are an exception, at least for now. At the end, all the above issues suggest that further studies and approaches are still needed in the future to achieve a comprehensive physical and numerical modelling of self-aerated air-water flows.

Declaration of competing interest

The authors declare that they have no known competing financial interests or personal relationships that could have appeared to influence the work reported in this paper.

Acknowledgements

The Authors acknowledge the very constructive comments from the reviewer. Carlo Gualtieri acknowledges past fruitful discussions on numerical simulation of hydraulic jump with Dr. Daniel Valero and Ing. Nicolò Viti. Hubert Chanson acknowledges the helpful discussions and interactions during more than 35 years of research on self-aerated flows with many colleagues, former students and current students, including Prof. Colin Apelt, Prof. Fabian Bombardelli, Prof. Daniel Bung, Dr Stefan Felder, Dr Carlos Gonzalez, Dr Xinqian (Sophia) Leng, Dr Youkai Li, Prof. Pierre Lubin, Prof. Jorge Matos, Dr Frédéric Murzyn Rui (Ray) Shi, Dr Luke Toombes, Dr Hang Wang, Dr Davide Wüthrich, and Dr Gangfu Zhang (in alphabetical order).

References

Alfonsi, G., 2011. On direct numerical simulation of turbulent flows. Appl. Mech. Rev. 64, 020802.
ASME, 2009. Perspective: journal of fluids engineering editorial policy statement on the control of numerical accuracy. J. Fluid Eng. 115, 339–340.
Balachandar, S., Eaton, J.K., 2010. Turbulent disperse multiphase flow. Annu. Rev. Fluid Mech. 42, 111–133.
Bayon, A., Valero, D., García-Bartual, R., Vallés-Morán, F.J., López-Jiménez, P.A., 2016. Performance assessment of Openfoam and Flow-3D in the numerical modeling of a low Reynolds number hydraulic jump. Environ. Model. Software 80, 322–335. https://doi.org/10.1016/j.envsoft.2016.02.018.
Bertrand, J., 1878. Sur l'homogénéité dans les formules de physique. Comptes Rendus 86 (15), 916–920.
Blocken, B., Gualtieri, C., 2012. Ten iterative steps for model development and evaluation applied to computational fluid dynamics for environmental fluid mechanics. Environ. Model. Software 33, 1–22. https://doi.org/10.1016/j.envsoft.2012.02.001.
Bombardelli, F.A., 2012. Computational multi-phase fluid dynamics to address flows past hydraulic structures. In: Matos, J., Pagliara, S., Meireles, I. (Eds.), *Proceedings Of 4th IAHR International Symposium On Hydraulic Structures Ishs2014*, Aprh – Associação Portuguesa Dos Recursos Hídricos [Portuguese Water Resources Association]. 9-11 February, Porto, Portugal, Keynote lecture, (Cd-Rom), p. 19.
Buckingham, E., 1914. On physically similar systems; illustrations of the use of dimensional equations. Phys. Rev. 4 (4), 345–376.
Bung, D.B., Valero, D., 2016a. Optical flow estimation in aerated flows. J. Hydraul. Res. IAHR 54 (5), 1–6. https://doi.org/10.1080/00221686.2016.1173600.
Bung, D.B., Valero, D., 2016b. Application of the Optical Flow Method to Velocity Determination in Hydraulic Structure Models. In: Crookston, B., Tullis, B. (Eds.), Proc. 6th IAHR Intl. Symp. Hydraulic Structures. 27-30 June, Portland Or, Usa, pp. 50–60. https://doi.org/10.15142/T3600628160853, 27-30 June, Portland OR, USA.
Camino, G.A., Zhu, D.Z., Rajaratnam, N., 2015. Flow observations in tall plunging flow dropshafts. J. Hydraul. Eng. ASCE 141 (No. 1). https://doi.org/10.1061/(Asce)Hy.1943-7900.0000939. Paper 06014020.
Carrillo, J.M., Castillo, L.G., Marco, F., García, J.T., 2020. Experimental and numerical analysis of two-phase flows in plunge pools. J. Hydraul. Eng. ASCE 146 (No. 6). https://doi.org/10.1061/(Asce)Hy.1943-7900.0001763. Paper 04020044.
Chanson, H., 1995. Air entrainment in two-dimensional turbulent shear flows with partially developed inflow conditions. Int. J. Multiphas. Flow 21 (6), 1107–1121. https://doi.org/10.1016/0301-9322(95)00048-3.
Chanson, H., 1997. Air Bubble Entrainment in Free-Surface Turbulent Shear Flows. Academic Press, London, Uk, p. 401.
Chanson, H., 2002a. An experimental study of roman dropshaft hydraulics. J. Hydraul. Res. IAHR 40 (1), 3–12. https://doi.org/10.1080/00221680209499868.
Chanson, H., 2002b. "An Experimental Study of Roman Dropshaft Operation: Hydraulics, Two-phase Flow, Acoustics." Report Ch50/02. Dept of Civil Eng., Univ. of Queensland, Brisbane, Australia, p. 99.
Chanson, H., 2004a. The Hydraulics of Open Channel Flow: an Introduction, second ed. Butterworth-Heinemann, Oxford, Uk, p. 630.
Chanson, H., 2004b. Hydraulics of rectangular dropshafts. J. Irrigat. Drain. Eng. ASCE 130 (6), 523–529.
Chanson, H., 2007a. Bubbly flow structure in hydraulic jump. Eur. J. Mech. B Fluid 26 (3), 367–384. https://doi.org/10.1016/j.euromechflu.2006.08.001.
Chanson, H., 2007b. Air entrainment processes in rectangular dropshafts at large flows. J. Hydraul. Res. IAHR 45 (1), 42–53.
Chanson, H., 2009. Turbulent air-water flows in hydraulic structures: dynamic similarity and scale effects. Environ. Fluid Mech. 9 (2), 125–142. https://doi.org/10.1007/s10652-008-9078-3.
Chanson, H., 2010. Convective transport of air bubbles in strong hydraulic jumps. Int. J. Multiphas. Flow 36 (10), 798–814. https://doi.org/10.1016/j.ijmultiphaseflow.2010.05.006.
Chanson, H., 2012. Advective diffusion of air bubbles in turbulent water flows. In: Gualtieri, C., Mihailović, D.T. (Eds.), Fluid Mechanics of Environmental Interfaces, second ed. CRC Press/Balkema, Leiden, The Netherlands, pp. 181–219.
Chanson, H., 2012a. Momentum considerations in hydraulic jumps and bores. J. Irrigat. Drain. Eng. ASCE 138 (4), 382–385. https://doi.org/10.1061/(Asce)Ir.1943-4774.0000409.
Chanson, H., 2013. Hydraulics of aerated flows: qui pro quo? J. Hydraul. Res. IAHR, Invited Vision Paper 51 (3), 223–243. https://doi.org/10.1080/00221686.2013.795917.
Chanson, H., Brattberg, T., 2000. Experimental study of the air-water shear flow in a hydraulic jump. Int. J. Multiphas. Flow 26 (4), 583–607. https://doi.org/10.1016/S0301-9322(99)00016-6.

Chanson, H., Gualtieri, C., 2008. Similitude and scale effects of air entrainment in hydraulic jumps. J. Hydraul. Res. IAHR 46 (1), 35–44. https://doi.org/10.1080/00221686.2008.9521841.

Chanson, H., Leng, X., Wang, H., 2021. Challenging hydraulic structures of the 21st century - from bubbles, transient turbulence to fish passage. J. Hydraul. Res. IAHR, Invited Vision Paper 59 (1), 21–35. https://doi.org/10.1080/00221686.2020.1871429.

Chanson, H., Lubin, P., 2010. Discussion of 'verification and validation of a computational fluid dynamics (CFD) model for air entrainment at spillway aerators. Can. J. Civ. Eng. 37 (1), 135–138. https://doi.org/10.1139/L09-133.

Chanson, H., Manasseh, R., 2003. "Air entrainment processes in a circular plunging jet. Void fraction and acoustic measurements. J. Fluid Eng. Trans. ASME 125 (5, Sept.), 910–921. https://doi.org/10.1115/1.1595672.

Chen, J., Katz, J., 2005. Elimination of peak-locking error in PIV analysis using the correlation mapping method. Meas. Sci. Technol. 16 (No. 8), 1605.

Chippada, S., Ramaswamy, B., Wheeler, M.F., 1994. Numerical simulation of hydraulic jump. Int. J. Numer. Methods Eng. 37, 1381–1397.

Cummings, P.D., Chanson, H., 1999. An experimental study of individual air bubble entrainment at a planar plunging jet. Chem. Eng. Res. Des. Trans. IChemE, Part A 77 (A2), 159–164. https://doi.org/10.1205/026387699525918.

Cushman-Roisin, B., Gualtieri, C., Mihailović, D.T., 2012. Environmental fluid mechanics: current issues and future outlook. In: Gualtieri, C., Mihailović, D.T. (Eds.), Fluid Mechanics of Environmental Interfaces, second ed. CRC Press/Balkema, Leiden, The Netherlands, pp. 3–17.

De Padova, D., Mossa, M., Sibilla, S., Torti, E., 2013. 3D SPH modeling of hydraulic jump in a very large channel. J. Hydraul. Res. IAHR 51, 158–173. https://doi.org/10.1080/00221686.2012.736883.

De Padova, D., Mossa, M., Sibilla, S., 2018. SPH numerical investigation of characteristics of hydraulic jumps. Environ. Fluid Mech. 18, 849–870.

Ding, Q., Zhu, D.Z., 2018. Flow regimes in a dropshaft with limited air supply. J. Hydraul. Eng. ASCE 144 (5). https://doi.org/10.1061/(ASCE)HY.1943-7900.0001455. Paper 06018006.

Elgobashi, S., 1991. Particle-laden turbulent flows: direct simulation and closure models. Appl. Sci. Res. 48, 301–314.

Ervine, D.A., Falvey, H.T., 1987. Part 2, Mar. 1987. Behaviour of Turbulent Water Jets in the Atmosphere and in Plunge Pools, 83. Proceedings of the Institution Civil Engineers, London, pp. 295–314. Discussion: Part 2, Mar.-June 1988, 85, pp. 359–363.

Ervine, D.A., Mckeogh, E.J., Elsawy, E.M., 1980. Effect of Turbulence Intensity on the Rate of Air Entrainment by Plunging Water Jets, vol. 2. Proceedings of the Institution Civil Engineers, June, pp. 425–445.

Gonzalez, A., Bombardelli, F.A., 2005. Two-phase-flow theoretical and numerical models for hydraulic jumps, including air entrainment. In: Proceedings of the 31st IAHR Congress, September 2005. IAHR, pp. 16–21. Beijing, China.

Gualtieri, G., Gualtieri, P., 2004. Turbulence-based models for gas transfer analysis with channel shape factor. Environ. Fluid Mech. 4 (No 3), 249–271. September 2004.

Gualtieri, G., Chanson, H., 2004. Analysis of air bubbles probability distribution functions in a large-size dropshaft. In: 3rd International Symposium on Two-phase Flow Modelling and Experimentation (ISTP 2004), 22/24, p. 2004. Pisa, Italy, September.

Gualtieri, G., Chanson, H., 2007. Experimental analysis of Froude number effect on air entrainment in hydraulic jumps. Environ. Fluid Mech. 7 (3, June 2007), 217–238. https://doi.org/10.1007/s10652-006-9016-1.

Gualtieri, G., Chanson, H., 2010. Effect of Froude number on bubble clustering in a hydraulic jump. J. Hydraul. Res. IAHR 48 (No. 4, August 2010), 504–508. https://doi.org/10.1080/00221686.2010.491688.

Gualtieri, G., Chanson, H., 2011. Bubble clustering in a large-size dropshaft. Comparative analysis of different cluster criteria. In: *Proc. 34th IAHR World Congress*, Brisbane, Australia, 26 June-1 July, Engineers Australia Publication, Eric Valentine, Colin Apelt, James Ball, Hubert Chanson, Ron Cox, Rob Ettema. George Kuczera, Martin Lambert, Bruce Melville and Jane Sargison Editors, pp. 2452–2459.

Gualtieri, G., Chanson, H., 2013. Interparticle arrival time analysis of bubble distributions in a dropshaft and hydraulic jump. J. Hydraul. Res. IAHR 51 (No. 3, June 2013), 253–264. https://doi.org/10.1080/00221686.2012.762430.

Halbronn, G., Durand, R., Cohen de Lara, G., 1953. Air Entrainment in Steeply Sloping Flumes. Proc. 5th IAHR Congress, IAHR-ASCE, Minneapolis, Usa, pp. 455–466.

Hamill, L., 1995. Understanding Hydraulics. Macmillan, London, Uk.

Hanratty, T.J., Theofanous, T., Delhaye, J.M., Eaton, J., Mclaughlin, J., Prosperetti, A., Sundaresan, S., Tryggvason, G., 2003. Workshop findings. Int. J. Multiphas. Flow 29, 1047–1059.

Henderson, F.M., 1966. Open Channel Flow. Macmillan Company, New York, Usa.

Hino, M., 1961. On the mechanism of self-aerated flow on steep slope channels. Applications of the statistical theory of turbulence. Proc. 9th IAHR Congress, Dubrovnick, Yugoslavia, pp. 123–132.

Hirt, C.W., Nichols, B.D., 2008. Volume of fluid (Vof) method for the dynamics of free boundaries. J. Comput. Phys. 39, 201–225.

Hohermuth, B., Schmocker, L., Boes, R., Vetsch, D.F., 2020. Numerical simulation of air entrainment in uniform chute flow. J. Hydraul. Res. IAHR. https://doi.org/10.1080/00221686.2020.1780492.

Jesudhas, V., Balachandar, R., Roussinova, V., Barron, R., 2018. Turbulence characteristics of classical hydraulic jump using des. J. Hydraul. Eng. ASCE 144 (6). https://doi.org/10.1061/(ASCE)HY.1943-7900.0001427. Paper 04018022.

Jesudhas, V., Balachandar, R., Wang, H., Murzyn, F., 2020. Modelling hydraulic jumps: IDDES versus experiments. Environ. Fluid Mech. 20, 393–413. https://doi.org/10.1007/s10652-019-09734-5.

Jevdjevich, V., Levin, L., 1953. Entrainment of air in flowing water and technical problems connected with it. In: Proc. *5th IAHR Congress*. IAHR-ASCE, Minneapolis, Usa, pp. 439–454.

Kiger, K.T., and Duncan, J.H. (2012). "Air-Entrainment Mechanisms in Plunging Jets and Breaking Waves." Annual Review of Fluid Mechanics, Vol. 44, pp. 563-596 (Doi: 10.1146/annurev-fluid-122109-160724).

Kobus, H., 1984. Local air entrainment and detrainment. In: Iahr, Esslingen, Germany, H., Kobus (Eds.), Proceedings International Symposium on Scale Effects in Modelling Hydraulic Structures, p. 10. Paper 4.10.

Kucukali, S., Chanson, H., 2008. Turbulence measurements in hydraulic jumps with partially-developed inflow conditions. Exp. Therm. Fluid Sci. 33 (1), 41–53. https://doi.org/10.1016/j.expthermflusci.2008.06.012.

Kundu, P., Cohen, I., Dowling, P., 2012. Fluid Mechanics, fifth ed. Academic Press, p. 891.

Leng, X., Chanson, H., 2020. Hybrid modelling of low velocity zones in box culverts to assist fish passage: why simple is better! River Res. Appl. 36 (9), 1765–1777. https://doi.org/10.1002/rra.3710. Review Paper.

Leng, X., Simon, B., Khezri, N., Lubin, P., Chanson, H., 2018a. CFD modelling of tidal bores: development and validation challenges. Coast Eng. J. 60 (4), 423–436. https://doi.org/10.1080/21664250.2018.1498211.

Leng, X., Chanson, H., Lubin, P., 2018b. Air bubble entrainment in breaking bores: physical and numerical CFD modelling. In: *Proceedings Of the 6th IAHR International Symposium On Hydraulic Structures ISHS 2018*, Aachen, Germany, 15-18 May, B.P. Tullis and D.B. Bung Editors, p. 11. https://doi.org/10.15142/T3fs9q.

Leng, X., Lubin, P., Chanson, H., Chanson, H., Brown, R., 2020. CFD modelling of surface wave breaking in a long channel. In: Proceedings of 22nd Australasian Fluid Mechanics Conference Afmc2020. December, Published by The University of Queensland, Brisbane, Australia, pp. 7–10. Invited plenary lecture paper, Paper 229, 4 pages, (DOI: 10.14264/852394c).

Liggett, J.A., 1994. Fluid Mechanics. Mcgraw-Hill, New York, Usa.

Lighthill, J., 1978. Waves in Fluids. Cambridge University Press, Cambridge, Uk, p. 504.

Lopes, P., Leandro, J., Carvalho, R.F., Bung, D.B., 2017. Alternating skimming flow over a stepped spillway. Environ. Fluid Mech. 17 (2), 303–322.

Lopez-Cuervo, S., 1985. Medina Az-Zahra Ingeniera Y Formas. Publicaciones del Ministerio de Obras Publicas y Urbanismo, Madrid, Spain169 (in Spanish).

López, D., Marivela, R., Garrote, L., 2010. Smoothed particle hydrodynamics model applied to hydraulic structures: a hydraulic jump test case. J. Hydraul. Res. IAHR 48 (1), 142–158. https://doi.org/10.1080/00221686.2010.9641255.

Lubin, P., Glockner, S., Chanson, H., 2009. Numerical simulation of air entrainment and turbulence in a hydraulic jump. In: Proc. Colloque Shf Modèles Physiques Hydrauliques: Outils Indispensables du Xxie Siècle?, 24–25 Nov. Société Hydrotechnique de France, Lyon, France, pp. 109–114.

Lubin, P., Glockner, S., Chanson, H., 2010a. Numerical simulation of a weak breaking tidal bore. Mech. Res. Commun. 37 (1), 119–121. https://doi.org/10.1016/j.mechrescom.2009.09.008.

Lubin, P., Chanson, H., Glockner, S., 2010b. Large eddy simulation of turbulence generated by a weak breaking tidal bore. Environ. Fluid Mech. 10 (5), 587–602. https://doi.org/10.1007/s10652-009-9165-0.

Lubin, P., Chanson, H., 2017. Are breaking waves, bores, surges and jumps the same flow? Environ. Fluid Mech. 17 (1), 47–77. https://doi.org/10.1007/s10652-016-9475-y.

Lubin, P., Glockner, S., 2015. Numerical simulations of three-dimensional plunging breaking waves: generation and evolution of aerated vortex filaments. J. Fluid Mech. 767, 364–393. https://doi.org/10.1017/jfm.2015.62.

Ma, J., Oberai, A.A., Lahey, R.T., Drew, D.A., 2011. Modeling air entrainment and transport in a hydraulic jump using two-fluid Rans and Des turbulence models. Heat Mass Tran. 47, 911.

Ma, Y., Zhu, D.Z., Rajaratnam, N., 2016. Air entrainment in a tall plunging flow dropshaft. J. Hydraul. Eng. ASCE 142 (10), 04016038. https://doi.org/10.1061/(ASCE)HY.1943-7900.0001181.

Macián-Pérez, J.F., Bayon, A., García-Bartual, R., López-Jiménez, P.A., Vallés-Morán, F. J., 2020. Characterization of structural properties in high Reynolds hydraulic jump based on CFD and physical modeling approaches. J. Hydraul. Eng. ASCE 146 (12). https://doi.org/10.1061/(ASCE)HY.1943-7900.0001820. Paper 04020079-4.

Mckeogh, E.J., Ervine, D.A., 1981. Air entrainment rate and diffusion pattern of plunging liquid jets. Chem. Engrg. Science 36, 1161–1172.

Meireles, I., Bombardelli, F.A., Matos, J., 2014. Air entrainment onset in skimming flows on steep stepped spillways: an analysis. J. Hydraul. Res. IAHR 52 (3), 375–385. https://doi.org/10.1080/00221686.2013.878401.

Mortazavi, M., Le Chenadec, V., Moin, P., Mani, A., 2016. Direct numerical simulation of a turbulent hydraulic jump: turbulence statistics and air entrainment. J. Fluid Mech. 797, 60–94. https://doi.org/10.1017/jfm.2016.230.

Murzyn, F., Chanson, H., 2009. Two-phase flow measurements in turbulent hydraulic jumps. Chem. Eng. Res. Des. Trans. IChemE, Part A 87 (6), 789–797. https://doi.org/10.1016/j.cherd.2008.12.2003.

Murzyn, F., Mouaze, D., Chaplin, J.R., 2005. Optical fibre probe measurements of bubbly flow in hydraulic jumps. Int. J. Multiphas. Flow 31 (1), 141–154.

Nikeghbali, P., Omidvar, P., 2017. Application of the SPH method to breaking and undular tidal bores on a movable bed. J. Waterw. Port, Coast. Ocean Eng. ASCE 144 (No. 2). https://doi.org/10.1061/(ASCE)WW.1943-5460.0000424. Paper 04017040.

Nobrega, J., Matos, J., Schultz, H.E., Canelas, R.B., 2020. Smooth and stepped spillway modeling using the SPH method. J. Hydraul. Eng. ASCE 146 (8). https://doi.org/10.1061/(ASCE)HY.1943-7900.0001776. Paper 04020054.

Novak, P., Cabelka, J., 1981. Models in Hydraulic Engineering. Physical Principles and Design Applications. Pitman Publ., London, Uk, p. 459.

Prosperetti, A., Tryggvason, G., 2009. Computational Methods for Multiphase Flows. Cambridge University Press, Uk, p. 469.
Rajaratnam, N., 1962. An experimental study of air entrainment characteristics of the hydraulic jump. J. Inst. Eng. India 42 (7), 247–273.
Rajaratnam, N., 1965. The hydraulic jump as a wall jet. J. Hydraul. Div. ASCE 91 (HY5), 107–132. Discussion: Vol. 92, No. Hy3, pp. 110–123 & Vol. 93, No. Hy1, pp. 74–76.
Rao, N.S.L., and Kobus, H.E. (1974). "Characteristics of Self-Aerated Free-Surface Flows." Water and Waste Water/Current Research and Practice, Vol. 10, Eric Schmidt Verlag, Berlin, Germany, 224 pages.
Rayleigh, Lord, 1915. The principle of similitude. Nature 95 (2368), 66–68.
Rizzi, A., Vos, J., 1998. Toward establishing credibility in computational fluid dynamics simulations. AIAA J. 36 (5), 668–675.
Roache, R.L., 1998. Verification of codes and calculations. AIAA J. 36 (5), 696–702.
Roache, P.J., 2008. Validation: definitions or descriptions?. In: Proc. 3rd Workshop on CFD Uncertainty Analysis. October, Lisbon, p. 5.
Rodi, W., 2017. Turbulence modeling and simulation in hydraulics: a historical review. J. Hydraul. Eng. ASCE 143 (No. 5), 20. https://doi.org/10.1061/(ASCE)HY.1943-7900.0001288. Paper 03117001.
Rodi, W., Constantinescu, G., Stoesser, T., 2013. Large-Eddy Simulation in Hydraulics. CRC Press, Boca Raton, Fl, Usa, p. 264.
Rouse, H., 1938. Fluid Mechanics for Hydraulic Engineers." Mcgraw-Hill Publ., New York, Usa, 1961. also Dover Publ., New York, Usa, p. 422.
Ryu, Y., Chang, K.A., Lim, H.J., 2005. Use of bubble image velocimetry for measurement of plunging wave impinging on structure and associated green water. Meas. Sci. Technol. 16 (10), 1945–1953.
Sousa, V., Bombardelli, F.A., Chanson, H., 2009. Numerical simulation of rectangular dropshafts using a Volume-of-Fluid (VoF) technique. In: Proc. 33rd IAHR World Congress, 2009. Canada, Vancouver. August, 10/14.
Toro, J.P., Bombardelli, F.A., Paik, J., Meireles, I., Amador, A., 2016. Characterization of turbulence statistics on the non-aerated skimming flow over stepped spillways: a numerical study. Environ. Fluid Mech. 16 (6), 1195–1221. https://doi.org/10.1007/s10652-016-9472-1.
Tryggvason, G., Scardovelli, R., Zaleski, S., 2011. Direct Numerical Simulations of Gas-Liquid Multiphase Flows. Cambridge University Press, Cambridge, Uk, p. 338.
Valero, D., Fullana, O., García-Bartual, R., Andrés-Domenech, I., Vallés-Morán, F.J., 2014. Analytical formulation for the aerated hydraulic jump and physical modelling comparison. In: Proc.: 3rd IAHR Europe Congress. Porto. Portugal.
Valero, D., Bung, D.B., Crookston, B.M., 2018. Energy dissipation of a Type Iii basin under design and adverse conditions for stepped and smooth spillways. J. Hydraul. Eng. 144 (7) https://doi.org/10.1061/(ASCE)HY.1943-7900.0001482. Paper 04018036.
Valero, D., Viti, N., Gualtieri, C., 2018. Numerical simulation of hydraulic jumps. Part 1: experimental results for performance assessment". Water, 2019 11 (No. 1), 36. https://doi.org/10.3390/w11010036. December 2018.
Vaschy, A., 1892. Sur les lois de similitude en physique. Annales Télégraphiques 19, 25–28 (in French).
Veron, F., 2015. Ocean spray. Annu. Rev. Fluid Mech. 47, 507–538. https://doi.org/10.1146/annurev-fluid-010814-014651.
Violeau, D., Rogers, B.D., 2016. Smoothed particle hydrodynamics (SPH) for free-surface flows: past, present and future. J. Hydraul. Res. IAHR 54 (1), 1–26. https://doi.org/10.1080/00221686.2015.1119209.
Viti, N., Valero, D., Gualtieri, C., 2018. Numerical simulation of hydraulic jumps. Part 2: recent results and future outlook. Water, 2019 11 (No. 1), 28. https://doi.org/10.3390/w11010028. December 2018.
Wan, H., Li, R., Gualtieri, C., Yang, H., Feng, J., 2017. Numerical simulation of hydrodynamics and reaeration over a stepped spillway by the SPH method. Water 9 (No. 8), 565. https://doi.org/10.3390/w9080565.
Wan, H., Li, R., Pu, X., Zhang, H., Feng, J., 2018. Numerical simulation for the air entrainment of aerated flow with an improved multiphase SPH model. Int. J. Comput. Fluid Dynam. 31 (10), 435–449. https://doi.org/10.1080/10618562.2017.1420175.
Wang, H., Chanson, H., 2015. Air entrainment and turbulent fluctuations in hydraulic jumps. Urban Water J. 12 (6), 502–518. https://doi.org/10.1080/1573062x.2013.847464.
Wang, H., Chanson, H., 2016. Self-similarity and scale effects in physical modelling of hydraulic jump roller dynamics, air entrainment and turbulent scales. Environ. Fluid Mech. 16 (6), 1087–1110. https://doi.org/10.1007/s10652-016-9466-z.
Wang, H., Hu, Z., Chanson, H., 2015a. Two-dimensional bubble clustering in hydraulic jumps. Exp. Therm. Fluid Sci. 68, 711–721. https://doi.org/10.1016/j.expthermflusci.2015.07.006.
Wang, H., Murzyn, F., Chanson, H., 2015b. Interaction between free-surface, two-phase flow and total pressure in hydraulic jump. Exp. Therm. Fluid Sci. 64, 30–41. https://doi.org/10.1016/j.expthermflusci.2015.02.003.
Wanninkhof, R., Asher, W.E., Ho, D.T., Sweeney, C., Mcgillis, W.R., 2009. Advances in quantifying air-sea gas exchange and environmental forcing. Annu. Rev. Fluid Mech. 1, 213–244.
Witt, A., Gulliver, J., Shen, L., 2018. Numerical investigation of vorticity and bubble clustering in an air entraining hydraulic jump. Comput. Fluids 172, 162–180. https://doi.org/10.1016/j.compfluid.2018.06.019.
Wood, I.R., 1984. Air entrainment in high speed flows. In: IAHR, Esslingen, Germany, H. Kobus (Eds.), Proc. International Symposium on Scale Effects in Modelling Hydraulic Structures. IAHR, p. 7 paper 4.1.
Wood, I.R., 1985. Air water flows. In: Proc. 21st IAHR Congress. IAHR, pp. 18–29. Melbourne, Australia, Keynote address.
Wood, I.R., 1991. Air entrainment in free-surface flows. In: *IAHR Hydraulic Structures Design Manual No. 4*, Hydraulic Design Considerations. Balkema Publ., Rotterdam, The Netherlands, p. 149.
Zhang, G., Chanson, H., Wang, H., 2016. Total pressure fluctuations and two-phase flow turbulence in self-aerated stepped chute flows. Flow Meas. Instrum. 51, 8–20. https://doi.org/10.1016/j.flowmeasinst.2016.08.007.
Zhang, G., Chanson, H., 2018. Application of local optical flow methods to high- velocity free-surface flows: validation and application to stepped chutes. Exp. Therm. Fluid Sci. 90, 186–199. https://doi.org/10.1016/j.expthermflusci.2017.09.010.

Further readings

Bahmanpouri, F., Gualtieri, C., Chanson, H., 2021. Flow patterns and free-surface dynamics in hydraulic jump on pebbled rough bed. In: Proceedings of the Institution of Civil Engineers – Water Management. https://doi.org/10.1680/jwama.20.00040 (in press).
Bombardelli, F.A., 2020. Seeing is believing: using hybrid turbulence closures to uncover the features of flows past hydraulic structures. In: Janssen, R., Chanson, H. (Eds.), *Proceedings Of 8th IAHR International Symposium On Hydraulic Structures Ishs2020*, Santiago, Chile, 12-15 May, the University of Queensland, Invited Plenary Lecture, p. 10. https://doi.org/10.14264/uql.2020.514.
Bradshaw, P., 1971. "An Introduction to Turbulence and its Measurement." Pergamon Press. The Commonwealth and International Library of Science and technology Engineering and Liberal Studies, Thermodynamics and Fluid Mechanics Division, Oxford, Uk, p. 218.
Felder, S., 2013. Air-Water Flow Properties on Stepped Spillways for Embankment Dams: Aeration, Energy Dissipation and Turbulence on Uniform, Non-uniform and Pooled Stepped Chutes. Ph.D. thesis. School of Civil Engineering, The University of Queensland, Brisbane, Australia.
Gerhart, P.M., Gross, R.J., Hochstein, J.I., 1992. Fundamentals of Fluid Mechanics, second ed. Addison-Wesley Publ., Reading Ma, Usa, p. 983.
Leng, X., 2018. A study of turbulence: the unsteady propagation of bores and surges. Ph. D. thesis. In: School of Civil Engineering & 2 Digital Appendices. The University of Queensland, Brisbane, Australia, p. 364. https://doi.org/10.14264/uql.2018.501.
Rouse, H., 1946. Elementary Mechanics of Fluids. John Wiley & Sons, New York, Usa, p. 376.
Rouse, H., 1959. Advanced Mechanics of Fluids. John Wiley, New York, Usa, p. 444.
Tennekes, H., Lumley, J.L., 1972. A First Course in Turbulence. Mit Press, Cambridge Ma, Usa, p. 300.
Toombes, L., 2002. Experimental Study of Air-Water Flow Properties on Low-Gradient Stepped Cascades. Ph.D. thesis. Dept of Civil Engineering, The University of Queensland, Brisbane, Australia.
Toro, J.P., Bombardelli, F.A., Paik, J., 2017. Detached eddy simulation of the nonaerated skimming flow over a stepped spillway. J. Hydraul. Eng. ASCE 143 (No. 9), 14. Paper 04017032.
Tryggvason, G., Scardovelli, R., Zaleski, S., 2011. Direct Numerical Simulations of Gas-Liquid Multiphase Flows. Cambridge University Press, Cambridge, Uk.
Valero, D., 2018. On the Fluid Mechanics of Self-Aeration in Open Channel Flows. Ph.D. thesis. University of Liège, Belgium, and Fh Aachen University of Applied Sciences, Germany.
Wang, H., 2014. Turbulence and Air Entrainment in Hydraulic Jumps. Ph.D. thesis. In: School of Civil Engineering & Digital Appendices. The University of Queensland, Brisbane, Australia, p. 341. https://doi.org/10.14264/uql.2014.542.
Zabaleta, F., Bombardelli, F.A., Toro, J.P., 2020. Towards an understanding of the mechanisms leading to air entrainment in the skimming flow over stepped spillways. Environ. Fluid Mech. 20, 375–392. https://doi.org/10.1007/s10652-019-09729-2.
Zhang, G., 2017. Free-Surface Aeration, Turbulence, and Energy Dissipation on Stepped Chutes with Triangular Steps, Chamfered Steps, and Partially Blocked Step Cavities. Ph.D. thesis. School of Civil Engineering, The University of Queensland, p. 361. https://doi.org/10.14264/uql.2017.906.